Case Study

# Case Study on the Impact of Horizontal Boundary Elements Design on Seismic Behavior of Steel Plate Shear Walls

Ronny Purba, S.M.ASCE[1]; and Michel Bruneau, F.ASCE[2]

**Abstract:** A case study was conducted to investigate the seismic behavior of steel plate shear walls having boundary elements designed by two different philosophies. The first design approach does not guarantee that formation of in-span plastic hinges on horizontal boundary elements (HBEs) will be prevented, whereas the second approach guarantees that plastic hinges can only occur at the ends of HBEs. Pushover and nonlinear time-history analyses were conducted to investigate behavior. Results show that the development of in-span plastic hinges has significant consequences on the behavior of the structure through inducing (1) significant accumulation of plastic incremental deformations on the HBEs; (2) partial yielding of the infill plates; (3) lower global plastic strength compared with values predicted by code equations; and (4) total (elastic and plastic) HBE rotations greater than 0.03 radians after the structure was pushed cyclically up to a maximum lateral drift of 3%. Nonlinear time-history analyses also demonstrated that increasing the severity of the ground excitations [i.e., from design basis earthquake (DBE) to maximum considered earthquake (MCE)] acting on the structure with in-span plastic hinge accentuated the accumulation of plastic incremental deformations on the HBEs. **DOI: 10.1061/(ASCE)ST.1943-541X.0000490.** © *2012 American Society of Civil Engineers.*

**CE Database subject headings:** Plastic hinges; Seismic effects; Steel plates; Shear walls; Deformation; Case studies.

**Author keywords:** In-span plastic hinge; Seismic behavior; Steel plate shear walls; Boundary elements design; Cumulative plastic incremental deformation.

## Introduction

Numerous experimental and analytical studies have investigated the behavior of unstiffened steel plate shear walls (SPSW) in the past thirty years. An AISC design guide summarizes the research (Sabelli and Bruneau 2007) that has addressed the designing and modeling of SPSW web plates, general SPSW analysis methods, validation of satisfactory cyclic inelastic and seismic performances, and analytical procedures to calculate demands in the horizontal and vertical boundary elements (HBEs and VBEs) of the SPSW (e.g., Thorburn et al. 1983; Timler and Kulak 1983; Caccese et al. 1993; Driver et al. 1997; Berman and Bruneau 2003, 2008; Qu et al. 2008, to name a few). As a result of this research, provisions for SPSW design have been adopted (e.g., AISC 2005), and they have been increasingly implemented in seismic regions.

The seismic behavior of SPSW has traditionally benefited from the overstrength introduced in the HBEs and VBEs of the boundary frame by capacity design principle requirements followed in previous research, but as practicing engineers are becoming more familiar with this structural system, they are finding ways to optimize the system and eliminate much of that overstrength to achieve smaller boundary element member sizes (Qu and Bruneau 2009). This can become problematic in light of the challenges that sometimes exist in deter-

mining satisfactory demands in designing the HBEs (e.g., Lopez-Garcia and Bruneau 2006; Qu et al. 2008; Vian and Bruneau 2005).

The 2005 AISC Seismic Provisions for Structural Steel Buildings (AISC 2005) requires that HBEs and VBEs be designed to remain essentially elastic under the maximum tension forces from the yielded infill plates, with the exception of plastic hinging at the ends of HBEs. However, the provisions do not specify an analysis procedure to guarantee that this intent is met (although the commentary provides some guidance that could be used for this purpose). As a result, at least two different common design approaches have been encountered in practice for which SPSWs are likely to develop in-span hinges. In a first approach, structural engineers typically use the results of an elastic analysis program and verify that the moments do not exceed the plastic moment capacity of the HBE. That by itself does not protect against in-span hinges. In the second approach, compounding on the first one, structural engineers seek to optimize the distribution of resistance to the lateral load between the boundary elements and infill plate, such as obtaining a boundary frame with the strength to resist its share of the lateral loads equal to that required to resist the demands from capacity design principles (i.e., attributable to the yielding plates), effectively eliminating the overstrength of the boundary frame (e.g., Qu and Bruneau 2009). In both cases, structural engineers might not anticipate that their design may lead to in-span HBE plastic hinges (unless these analyses are complemented by the use of nonlinear analysis programs to predict the plastic mechanism of structures). In parallel, some structural engineers fully recognize the potential for in-span hinging to develop but question the merit of limiting the location of plastic hinges to only occur at the ends of HBEs because, in general, this design requirement results in a relatively substantial size of boundary elements. Thus, to achieve more economical designs, structural engineers are attempting to minimize overstrength by allowing plastic hinges

[1]Graduate Research Assistant, Dept. of CSEE, Univ. at Buffalo, Amherst, NY 14260 (corresponding author). E-mail: rpurba@buffalo.edu

[2]Professor, Dept. of CSEE, Univ. at Buffalo, Amherst, NY 14260. E-mail: bruneau@buffalo.edu

to occur along the HBE span, as this leads to relatively smaller boundary elements. Whether this is acceptable has been a contentious issue, particularly in the absence of factual data.

To investigate this concern, one must first determine whether in-span HBE hinging, when it occurs, can affect in any way the seismic performance of SPSWs, irrespective of whether it develops intentionally in a SPSW or as a result of unintended design consequences. This paper presents an investigation of the question using a case study for this purpose. Undoubtedly, subsequent research and parametric studies would be useful to identify the specific conditions and wall geometries (e.g., aspect ratios, number of stories) for which specific behaviors would be obtained to quantify their likelihood of occurrence and to determine whether other attenuating factors can be relied on to counter potential undesirable behaviors. However, an understanding of the possible consequences of in-span HBE plastic hinging is a prerequisite for any such further questioning. In that perspective, whereas overstrength in SPSWs is recognized to arise from a number of sources during design, the case study presented has been careful to ensure that its conclusions are not biased by accidental sources of overstrength that may or may not be present from case to case. Future analysis would allow quantification and assessment of the reliability of various sources of uncontrolled overstrength.

Hence, to answer the fundamental question in this debate, this paper presents the results of a case study that analytically investigated the seismic behavior of two steel plate shear walls having HBEs designed with different plastic mechanisms. In the first SPSW, one of the preceding design approaches is used and formation of in-span plastic hinges on HBEs is possible, whereas in the second SPSW, plastic hinges can only occur at the ends of HBEs. Results and observations from monotonic and cyclic pushover analyses and time-history analyses are used to assess the relative performance of the two SPSWs.

## Structure Description and Design of Three-Story SPSW

As a case study to investigate the possible significance of in-span HBE plastic hinges, a three-story single-bay SPSW was selected. Bay width and typical story height were arbitrarily chosen equal to 20 and 10 ft, respectively, resulting in an infill plate aspect ratio of 2.0. Note that SPSWs having such an aspect ratio are common nowadays (e.g., AISC 2007, 2008) and that larger values are anticipated as the 2010 edition of the AISC seismic provisions (AISC 2010) has eliminated the previously prescribed upper limit for that ratio. It was also assumed that the structure is located on Class D soil in downtown San Francisco, California, and designed for an office building. This SPSW was assumed to carry a tributary weight $W_t$ of 1085 kips, which corresponds to one-sixth of the total weight of the structure, distributed as 352 kips on the first two stories and 381 kips on the roof. Different approaches were possible to ensure that the strength of the chosen web plates closely matched the design demands (to avoid having infill plate overstrength bias the findings of this study). For example, (1) the SPSW's tributary mass could have been modified to match the strength of available hot rolled plates, (2) regular perforation layouts in compliance with the AISC 341-10 requirements for Special Perforated Steel Plate Walls (AISC 2010) could have been detailed, or (3) cold rolled steel plates could have been used. Given that all of these approaches would lead to the same end results, for expediency the later approach was taken, knowing that satisfactory ductile behavior of SPSWs having such infill plates can be obtained (Berman and Bruneau 2005). Thus, light-gauge steel ($F_y = 30$ ksi) was used

for the infill plates. ASTM A572 Gr. 50 ($F_y = 50$ ksi) steel was selected for the VBEs and HBEs.

On the basis of the spectral acceleration maps in *FEMA Report No. 450* (2003) provisions, the design short and 1-second spectral ordinates, $S_{DS}$ and $S_{D1}$, for the aforementioned site are 1.14 $g$ and 0.85 $g$, respectively. The fundamental period of the structure $T$ was estimated using the *FEMA Report No. 450* (2003) procedures as 0.26 s, and using a response modification factor $R$ of 7 and an importance factor $I$ of 1, the total base shear $V$ resisted by the structure was 176 kips, distributed as lateral loads along the height of the building of 92, 56, and 28 kips from the third to the first floor. The required infill plate thicknesses to resist those story shear forces per Eq. 17-(1) of the AISC 2005 Seismic Provisions were 0.072, 0.059, and 0.036 in. for the first to the third floor, respectively. Those exact thicknesses were assumed to be available (slightly thicker plates would have imparted greater demands on the HBEs but would not have significantly changed the observed behavior described in subsequent sections). Two design procedures were applied to design the boundary elements.

### Indirect Capacity Design Approach

According to the indirect capacity design approach, described in the commentary to the AISC seismic provisions (AISC 2005, 2010), loads in the boundary elements can be determined from the gravity loads combined with equivalent seismic loads increased by the amplification factor

$$B_i = \frac{V_{ei}}{V_{ui}} \tag{1}$$

where $V_{ei}$ = expected shear strength calculated for the infill plate thickness provided and $V_{ui}$ = lateral seismic force at floor $i$. Following this procedure, a linear analysis program is typically used to analyze the SPSW and size of the boundary elements. SAP2000 software (SAP2000 Version 11.0.8) was used to design the VBEs and HBEs with the objective of obtaining a demand-to-capacity ratio close to 1.0 (without exceeding it) when resisting the combination of gravity loads and earthquake loads increased by the amplification factor $B_i$.

### Combined Plastic and Linear Analysis (Capacity Design)

The capacity design approach used combines the procedure proposed by Vian and Bruneau (2005) for HBEs and that proposed by Berman and Bruneau (2008) for VBEs. The latter procedure is also described in the commentary to the 2010 AISC seismic provisions (AISC 2010).

Vian and Bruneau (2005) proposed an equation to size anchor beams (i.e., top and bottom HBEs) such that they can resist forces generated by fully yielding infill plates without developing in-span HBE plastic hinges. The equation estimates the minimum required HBE plastic modulus as follows:

$$Z_i = \frac{\omega_{ybi}L_b^2}{4 \, F_{yb}} \tag{2}$$

where $L_b$ and $F_{yb}$ = HBE span and yield stress, respectively and $\omega_{ybi}$ = vertical component of infill plate stress, defined as

$$\omega_{ybi} = F_{yp} \, t_{pi} \cos^2\alpha \tag{3}$$

where $F_{yp}$ and $t_{pi}$ = infill plate yield stress and infill thickness, respectively, and $\alpha$ = tension field inclination angle. Although Eq. (2) was developed for anchor beams, it can also be applied to the design of intermediate HBEs by considering the net stress

resulting from the adjacent top and bottom infill plates of different thicknesses. As for VBEs, the Berman and Bruneau (2008) procedures derive their design loads from the free-body diagrams of the SPSW uniform plastic sway mechanism (i.e., full web yielding and plastic hinge at HBE ends).

The resulting sizes of VBEs and HBEs obtained by the two different design procedures are compared in Fig. 1. Note that the selected sections might not be the lightest W-section available and that the VBE section is again varied from floor to floor to ensure that the following observations are not tainted by accidental overstrengths. The demand-to-capacity ratio for each element is displayed in parentheses under the resulting section shape in Fig. 1. For SPSW designed by the capacity approach, all HBE demand-capacity ratios exceed 0.98 except one at 0.95. For SPSW designed by the indirect capacity approach, the HBE ratios varied from 0.88 to 0.99; however, this slight difference from the second SPSW case will not violate the conclusions reached by this study, as is shown subsequently. Moreover, the SPSWs resulting from the first and second design approach are denoted as SPSW-ID and SPSW-CD, respectively, where the ID and CD labels stand for "indirect design" and "capacity design," respectively. Note that the resulting observations on the behavior of SPSW-ID are equally applicable to SPSWs designed by any method for which in-span plastic hinges are not explicitly prevented.

## Analytical Model Development

To investigate the behavior of both SPSW-ID and SPSW-CD, nonlinear static analysis (pushover analysis) and time-history analysis were conducted. Two analytical models were developed for this purpose: (1) a strip model for monotonic pushover analysis and (2) a dual strip model for cyclic pushover analysis and time-history analyses. The second model can capture reorientation of the tension field direction as loading direction changes. The validity of such strip models to accurately capture the nonlinear behavior of SPSWs is well established (e.g., Driver et al. 1997, 1998; Elgaaly 1998; Berman and Bruneau 2003, 2005; Qu and Bruneau 2008). In this study, 12 strips having an equal width $S$ of 19.7 in. were provided at every floor to model the infill plates of the two three-story SPSWs discussed in the previous section. In SAP2000, those strips were modeled as series of tension-only bracing element, which has strength only in tension but no strength in compression (as commonly done in such SPSW inelastic analyses) and were inclined in the direction of the tension field $\alpha$ estimated per Eq. 17-(2) of the AISC 2005. For modeling expediency, a single inclination angle of 42° taken as the average tension field angle of all panels in SPSW-ID was used throughout the analytical model. As for the VBEs and HBEs, they were modeled as a regular frame element. ASTM A572 Gr. 50 steel and light gauge steel used for frame element and tension-only bracing element, respectively, were represented by an idealized elasto-perfectly plastic stress-strain material (i.e., no strain hardening included, as conventionally done using simple plastic theory).

To capture the nonlinear behavior of the structure, nonlinear hinges (plastic hinges) were also defined in the analytical models. Preliminary nonlinear static analyses demonstrated that for SPSW-ID, plastic hinges would develop at the ends of the HBEs and somewhere along their span, whereas they only occurred at the HBE ends for SPSW-CD. Hence, to develop a general model and expedite the modeling process for both the monotonic and cyclic pushover analyses, plastic hinge elements were defined at the quarter-, mid-, and third-quarter span of each HBE, in addition to their ends. One might argue that introducing more plastic hinge elements along the HBE span (e.g., every one-tenth of the HBE length) would have allowed closer approximation of the exact location of the plastic hinges and thus give a more precise estimate of the SPSW ultimate strength. However, this additional computational expense would only lead to marginal benefits, as known from a study of plastic mechanism under uniformly distributed loads
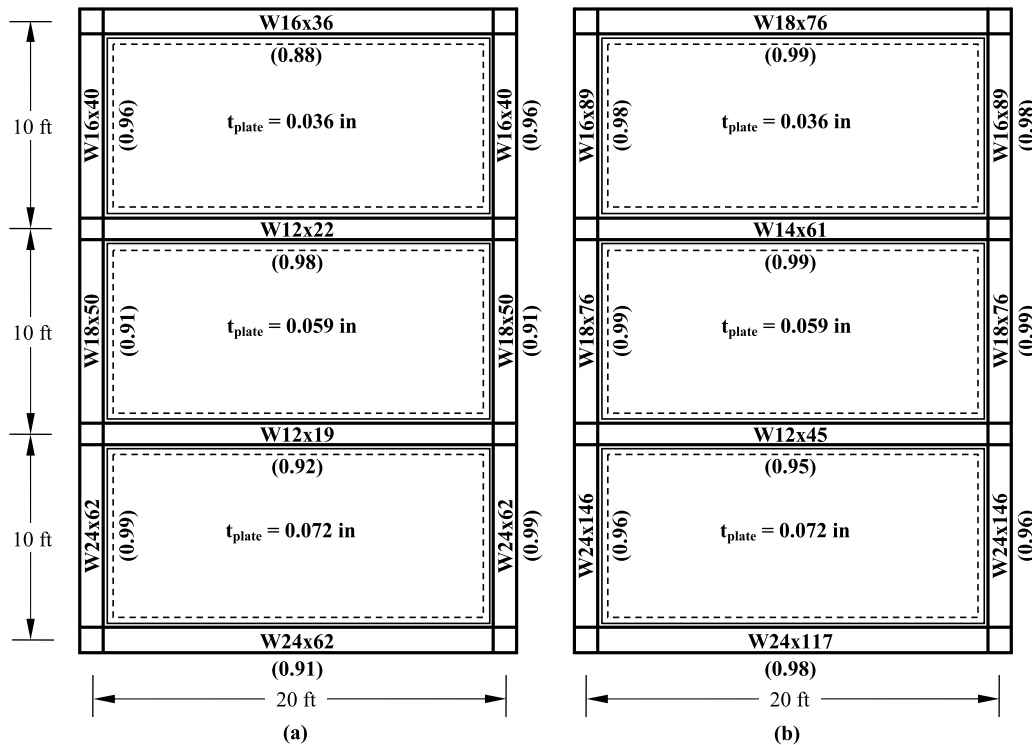


Fig. 1. VBE and HBE sizes with demand-to-capacity ratio results: (a) SPSW-ID; (b) SPSW-CD

(e.g., Bruneau et al. 1998), recognizing that the distributed tension loads from the infill plates act as a distributed load on the HBEs. In addition, to capture yielding of strips, axial hinges (i.e., understood as member-yielding under tension forces) were located at every tension strip over the entire stories. The SAP2000 axial-P hinge (configured and verified to exhibit correct hysteretic tension-only behavior) was chosen to define the inelastic behavior of the strips. The fiber P-M2-M3 hinge was chosen to define plastic hinges in the VBEs and HBEs. This type of hinge automatically accounts for the interaction between the axial loads and moments that can occur in the HBEs and VBEs (SAP2000).

## Nonlinear Static Analysis (Pushover Analysis)

### Monotonic Pushover Analysis

A monotonic pushover analysis was conducted for both SPSW-ID and SPSW-CD until each structure reached a 4% lateral drift, which corresponds to a 14.4 in. roof lateral displacement. The inverted triangular vertical distribution presented in the *FEMA Report No. 450* (2003) document was chosen to model the distribution of lateral loads along the height of the building. Lateral forces acting at every floor level were assumed to be transferred equally to the left and right sides of the SPSWs.

Fig. 2 shows the monotonic pushover results for both SPSW-ID and SPSW-CD. At 4% drift, the base shears are 311 and 477 kips for the respective structures; for comparison, their respective theoretical values (indicated in the figure by the dash lines) are 351 and 488 kips, obtained using the plastic analysis equations for uniform plastic sway mechanism (Berman and Bruneau 2003). As shown in Fig. 2 for SPSW-CD, the base shear obtained from the monotonic pushover analysis using SAP2000 and the theoretical calculations using the plastic analysis approach are in a good agreement. The difference between the two is only 2.3% at 4% drift. Several factors, such as fiber-hinge model properties, effect of axial forces, and actual tension field angle contributed to this small discrepancy (each of these effects is quantified in Purba and Bruneau 2010 and verified to add up to match the observed difference). However, for SPSW-ID, the theoretical base shear is 13% more than that obtained from the monotonic pushover analysis. Even if the factors that accounted for the discrepancy of results in SPSW-CD are applied to this condition, an 11% disparity remains, which can only be
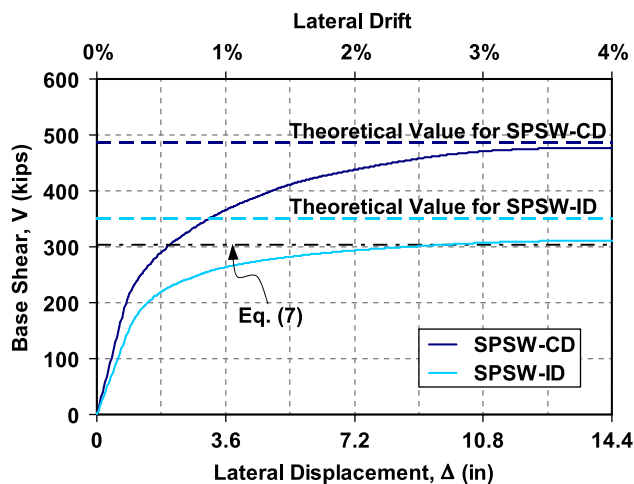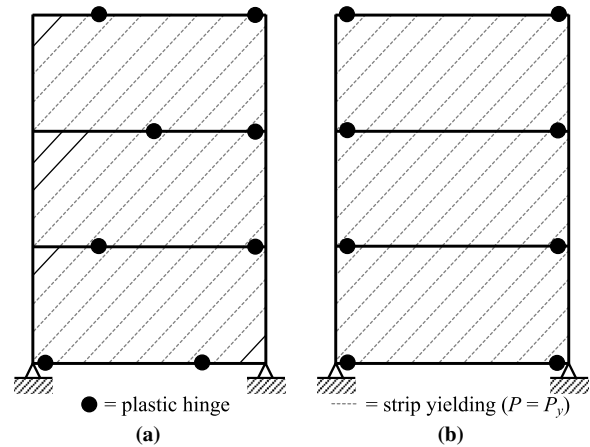


**Fig. 3.** Plastic hinge and strip yielding distributions at 3 and 4% lateral drift: (a) SPSW-ID; (b) SPSW-CD

explained by comparing the plastic mechanism from the SAP2000 analyses with the assumed theoretical one.

Fig. 3 displays plastic hinge and strip yielding distributions at 3% lateral drift for SPSW-ID and SPSW-CD, in which strip yielding is shown as broken lines, and where the circular markers indicate that a fully plastic condition has been reached on the HBE at each selected location. The same distributions are also observed at 4% lateral drift. As shown in Fig. 3(a), five out of 36 strips in SPSW-ID remained elastic, and four out of eight HBE ends did not develop plastic hinges. In contrast to the assumed uniform plastic sway mechanism described in the commentary to the AISC seismic provisions (2010), four in-span plastic hinges have developed on the HBEs of SPSW-ID. Hence, SPSW-ID certainly does not follow the uniform plastic sway mechanism (also known as panel mechanism) but rather consists of a sway and beam combined mechanism. The significant vertical deformations along the HBEs spans of SPSW-ID (as discussed subsequently in the "HBE Vertical Deformation" subsection) confirm development of this mechanism. For example, on the second- and top-floor HBEs, vertical deformations observed at their span are 4.3 and 2.4 inches at 4% drift, respectively. In comparison, all strips in SPSW-CD yielded and plastic hinges occurred at each HBE end (i.e., total of eight plastic hinges). Although the fiber-hinge elements were also present along the HBE span of SPSW-CD (at the same locations as for the SPSW-ID case), no in-span plastic hinge developed. This confirms that SPSW-CD follows a uniform plastic sway mechanism.

An equation to calculate the theoretical base shear strength of SPSW having in-span plastic hinges considering their actual plastic mechanism is derived in Appendix I. Eq. (7) in that appendix gives a theoretical base shear of 304 kips for SPSW-ID, which agrees to within 2.2% with the aforementioned 311 kips result from the SAP2000 analysis as shown in Fig. 2. The plastic mechanism considered in Appendix I is general and could develop in SPSWs having any number of stories.

### Cyclic Pushover Analysis

To investigate whether plastic hinging along an HBE span could lead to progressively increasing deformations in the HBEs of both SPSW-ID and SPSW-CD and whether it may affect structural performance, cyclic pushover analysis was conducted. A progressively increasing cyclic displacement history of up to 3% drift (in increments of 0.5%) was applied to the top floor of the structure for this purpose. In this paper, positive pushover displacement (producing
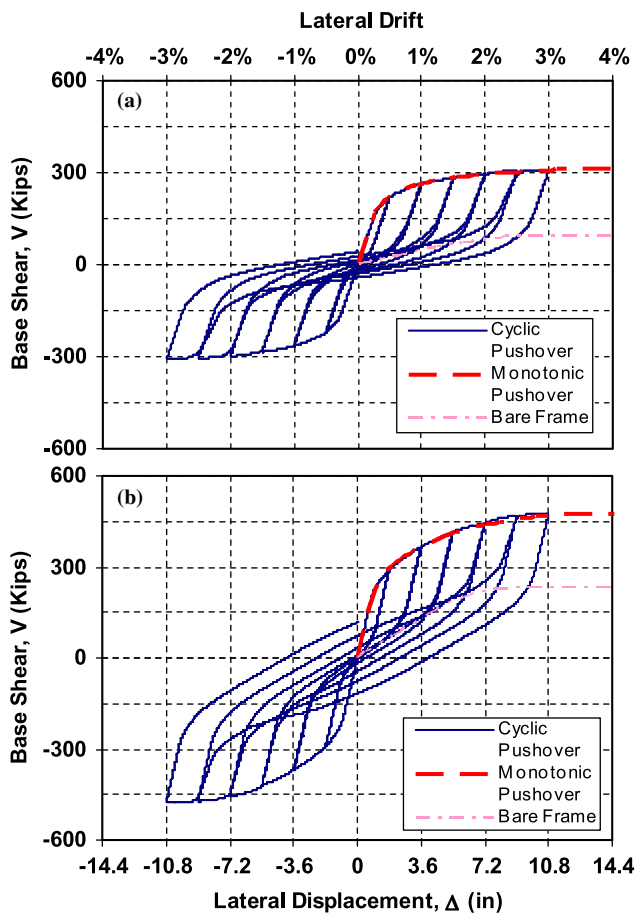


**Fig. 2.** Monotonic pushover analysis results

**Fig. 4.** Cyclic pushover analysis results: (a) SPSW-ID; (b) SPSW-CD

positive base shear) is assumed to be acting from left to right of the structure.

The resulting hysteretic curves of the base shear versus lateral displacement up to 3% drift for SPSW-ID and SPSW-CD are compared in Fig. 4. As shown in Fig. 4, the backbone of both cyclic pushover analyses follows the monotonic curves without significant differences. The boundary frame plastic strength (in a sway mechanism) was observed to contribute approximately 30 and 48% of the total plastic strength of SPSW-ID and SPSW-CD, respectively. This explains why SPSW-ID exhibits more pinching in its hysteretic behavior than SPSW-CD.

**Plastic Hinge and Strip Yielding Distributions.** To observe the progression of plastification at several drifts of interest during the cyclic pushover analysis, three stages of plastification have been defined: yielding condition, partial plastification condition, and fully plastic condition. The criterion used to define them is from the level of flexural moment (when the magnitude of axial force does not exceed what could be considered a moderate level, a limit defined as $P \leq 10\% P_y$) or from fiber stress-strain information (when the magnitude of axial forces developed in one particular fiber-hinge becomes significant, $P \geq 10\% P_y$). Using the second criterion, the yield condition corresponds with the stage for which the furthest fiber from the plastic neutral axis reaches the yield stress, extending that initial condition up to the upper boundary defined by the case for which all fibers on one flange yielded (i.e., per the first criterion, the flexural moment is between 88 and 91% of its theoretical plastic moment); the fully plastic condition corresponds with the instance for which most of the fibers yielded only one or two fibers close to the plastic neutral axis

remaining elastic (i.e., the flexural moment is equal to or higher than 97% of its theoretical plastic moment); and the partial plastification condition corresponds with the cases between those two conditions (i.e., for first criterion, the flexural moments is between 91 and 97% of its theoretical plastic moment).

Fig. 5(a) shows the plastic hinge and strip yielding distributions on SPSW-ID. Plotted from left to right are the conditions at the end of the full cycle at 1, 2, and 3% drift, respectively. To gain a better understanding of the plastic hinges formed in each direction of the pushover displacement, new markers were introduced in the figure, which are different from the one shown in Fig. 3 for monotonic pushover analysis. Symbolic hinges that are half-shaded or half-solid on the top part of the circular markers indicate that partial plastification or full plastic condition, respectively, was reached on the HBE at the shown location when the structure undergoes positive drift excursion. When the structure undergoes an excursion in the reversed direction, those half-shaded or half-solid indications are shown on the bottom part of the circular markers to indicate the same respective conditions. Consequently, full-shaded or full-solid indicate that the respective conditions occurred in both directions (i.e., positive and negative directions).

Fig. 5(a) shows that the plastic hinge distribution at the end of the 1% drift cycle is somewhat symmetric in both directions. When the structure experienced +1% lateral drift, a total of four plastic hinges (one partial plastification and three fully plastic) occurred at the HBE ends; and at the reversed excursion of −1% lateral drift, a total of five plastic hinges (two partial plastification and three fully plastic) occurred at the same HBE ends. In addition, three strips (the right-leaning or left-leaning strips for the positive or negative direction, respectively) on the second and the third floor remained elastic (shown as the solid lines close to the corner in the figure) and only two strips on the first floor had yielded (shown as the broken lines in the figure).

As the pushover displacement increased, more strips yielded, predominantly on the first floor, whereas only one additional strip yielded on the top floor. As previously observed in the monotonic pushover analysis, even at higher lateral drifts some strips remained elastic (i.e., a total of nine right-leaning strips and 10 left-leaning strips at the end of the 3% drift cycle). This phenomenon will be explained in the next section. Moreover, for the plastic hinge distribution, beyond the plastic hinges that occurred at the HBE ends, three locations of in-span plastic hinges were also observed on HBE2 (the second floor) and HBE3 (the third floor) at the end of 2% drift cycle. In addition, the yielding condition occurred along the span of HBE0 (on the ground floor) and HBE1 (on the first floor). At the end of the 3% drift cyclic, in-span plastic hinges on the HBEs occurred at four locations (one partial plastification and three fully plastic) during the positive drift excursion and at four locations (two for each partial plastification and fully plastic) during the negative drift excursion.

Incidentally, one interesting behavior observed on the plastic hinge distribution of SPSW-ID after the structure experienced a higher drift (i.e., $\geq 2\%$ drift) was evidence of three plastic hinges having formed in some of the HBEs. For example, this was observed on HBE2 when the structure underwent its positive drift excursion during the 2% drift cycle and on each HBE in both excursion directions of the 3% drift cycle. This behavior seems to contradict the results obtained for the theoretical sway and beam combined mechanism observed under monotonic pushover analysis illustrated and further discussed in Appendix I, in which only two plastic hinges on the HBEs were required to form the plastic mechanism; however, no contradiction exists. Purba and Bruneau (2010) comprehensively explained this phenomenon by conducting a step-by-step investigation on the free-body diagram of the
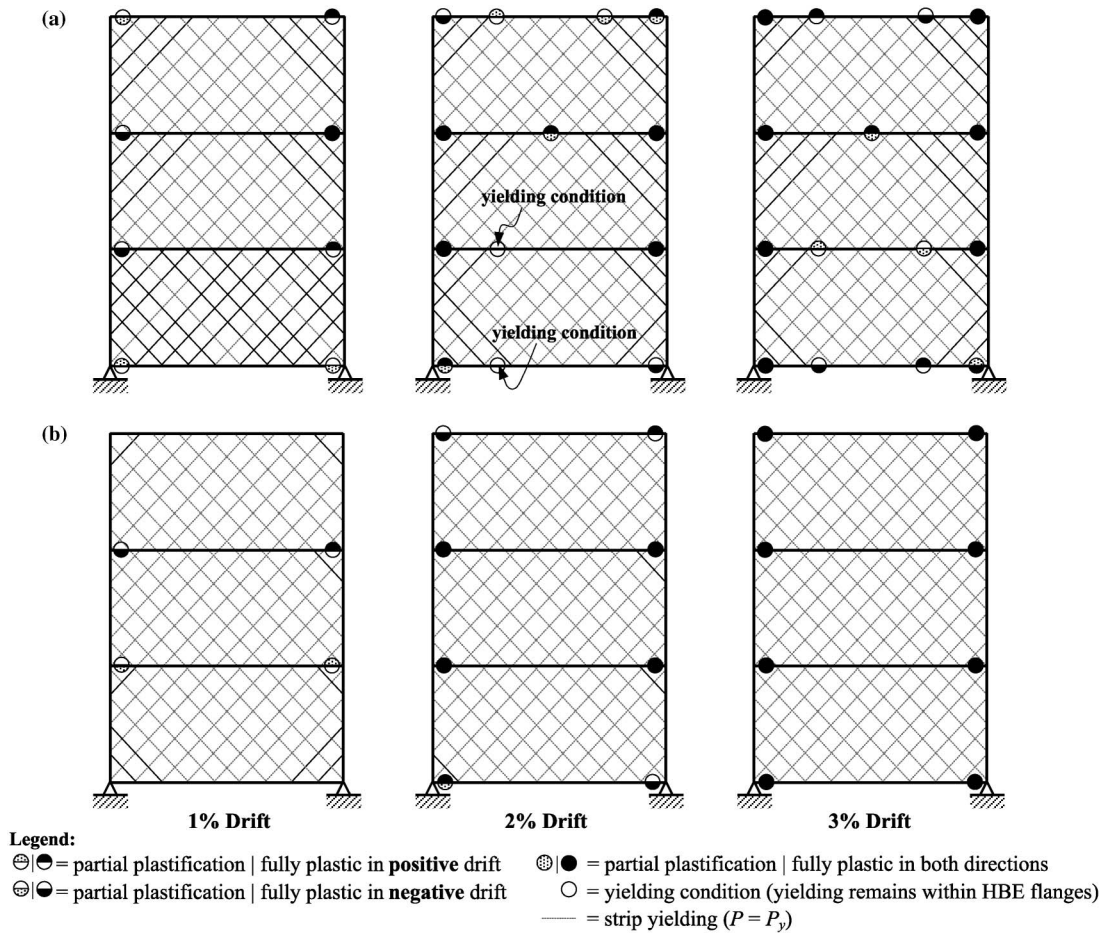
**Fig. 5.** Plastic hinge and strip yielding distributions on (a) SPSW-ID; (b) SPSW-CD

corresponding HBE (e.g., HBE3) during the 3% drift cycle. At the beginning of this cycle, after the structure was pushed to the right and to the left up to a maximum lateral drift of 2.5%, residual moments were observed at both ends of HBE3 and no tension forces remained in the strips because their elongations were less than the previous maximum elongation. As a result, at an earlier stage of pushover displacement during the 3% drift cycle, SPSW-ID behaves similar to a moment-resisting frame, with plastification concentrated at both HBE ends. However, as the strips regained tension at a higher drift and resumed plastic energy dissipation anew, the left end moment reduced during positive drift excursion whereas moments at the quarter-span from the left and at the right end increased. Eventually, the plastic hinge that occurred at the left end during increasing positive drifts was under elastic unloading and thus not plastic anymore. Instead, plastic hinges were located at the quarter-span from the left and at the right end of HBE3, similar to the observation in the monotonic pushover analysis case. The same behavior was also observed during the negative drift excursion where the location of the plastic hinges mirrors that in the positive drift excursion. Hence, this distinctive transition mechanism between the sway and the combined mechanism in SPSW-ID explains the plastic hinge distribution observed on its HBEs shown in Fig. 5(a). At the end of the cyclic pushover analysis, three plastic hinges indeed developed on those HBEs but they did not occur at the same time during the drift excursion. A small drop of HBE end moment at a higher drift after the infill plates yielded actually also occurred in several HBEs of SPSW-CD. However, changing of the

plastic hinge distribution did not follow (i.e., the system remained in its sway plastic mechanism), as opposed to the case of SPSW-ID.

Fig. 5(b) shows the plastic hinge strip yielding distributions on SPSW-CD. At the end of the 1% drift cycle, most of the strips yielded; only four right-leaning strips and five left-leaning strips (i.e., close to corners) remained elastic. In contrast to SPSW-ID, for the SPSW-CD, all strips completely yielded at the end of the 3% drift cycle. In addition, all plastic hinges developed at the HBE ends and no in-span plastic hinge developed.

**HBE Vertical Deformation.** A most significant phenomenon observed is the HBE vertical downward deformation of SPSW-ID, progressively increasing and of significant magnitude as the lateral drift increased. This can be observed especially on the top two HBEs, as shown in Fig. 6(a). For example, the vertical deformation on the top HBE progressively increased from 0.8 to 2.3 in. when the structure was pushed from 1 to 3% drift. Additionally, when the structure returned to its original position after it went through a full 3% drift cycle, the residual vertical deformation of the top HBE remained significant at approximately 1.7 in. (shown in Fig. 7). This significant HBE vertical deformation prevented the corner strips (i.e., the top left corner on the second and the third floor for positive pushover displacement and both strips on the top left and bottom right corners on the first floor) to completely stretch up to the yield displacement. This further explains why in Fig. 5 those corner strips remained elastic and in-span hinges developed. As a consequence of this behavior, the infill plates in SPSW-ID did not develop their full capacity to resist the specified lateral loads. By comparison, for SPSW-CD, relatively small vertical deformations
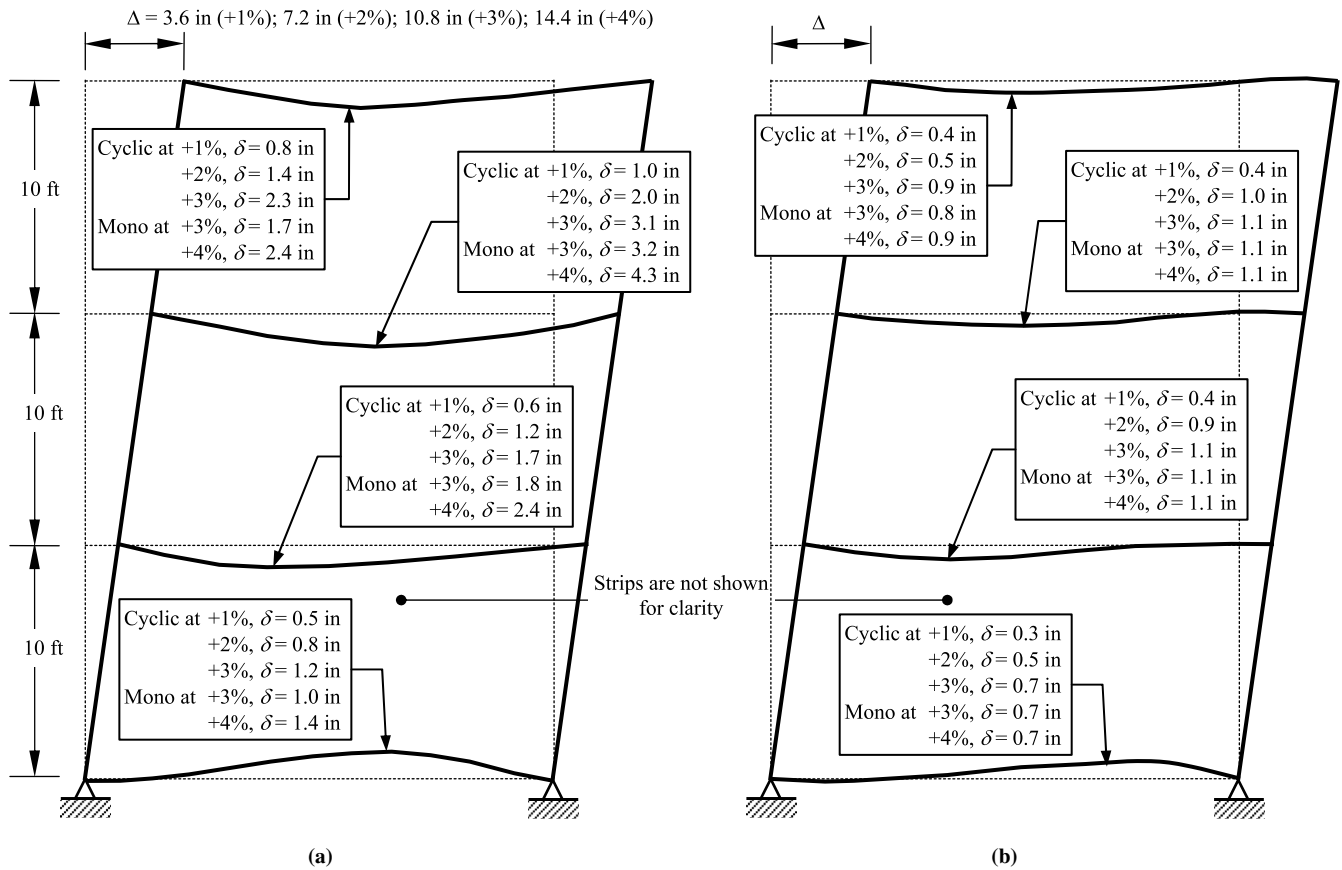
$\Delta = 3.6$ in ($+1\%$); 7.2 in ($+2\%$); 10.8 in ($+3\%$); 14.4 in ($+4\%$)

**(a)**

Cyclic at $+1\%$, $\delta = 0.8$ in
$+2\%$, $\delta = 1.4$ in
$+3\%$, $\delta = 2.3$ in
Mono at $+3\%$, $\delta = 1.7$ in
$+4\%$, $\delta = 2.4$ in

Cyclic at $+1\%$, $\delta = 1.0$ in
$+2\%$, $\delta = 2.0$ in
$+3\%$, $\delta = 3.1$ in
Mono at $+3\%$, $\delta = 3.2$ in
$+4\%$, $\delta = 4.3$ in

Cyclic at $+1\%$, $\delta = 0.6$ in
$+2\%$, $\delta = 1.2$ in
$+3\%$, $\delta = 1.7$ in
Mono at $+3\%$, $\delta = 1.8$ in
$+4\%$, $\delta = 2.4$ in

Cyclic at $+1\%$, $\delta = 0.5$ in
$+2\%$, $\delta = 0.8$ in
$+3\%$, $\delta = 1.2$ in
Mono at $+3\%$, $\delta = 1.0$ in
$+4\%$, $\delta = 1.4$ in

**(b)**

Cyclic at $+1\%$, $\delta = 0.4$ in
$+2\%$, $\delta = 0.5$ in
$+3\%$, $\delta = 0.9$ in
Mono at $+3\%$, $\delta = 0.8$ in
$+4\%$, $\delta = 0.9$ in

Cyclic at $+1\%$, $\delta = 0.4$ in
$+2\%$, $\delta = 1.0$ in
$+3\%$, $\delta = 1.1$ in
Mono at $+3\%$, $\delta = 1.1$ in
$+4\%$, $\delta = 1.1$ in

Cyclic at $+1\%$, $\delta = 0.4$ in
$+2\%$, $\delta = 0.9$ in
$+3\%$, $\delta = 1.1$ in
Mono at $+3\%$, $\delta = 1.1$ in
$+4\%$, $\delta = 1.1$ in

Cyclic at $+1\%$, $\delta = 0.3$ in
$+2\%$, $\delta = 0.5$ in
$+3\%$, $\delta = 0.7$ in
Mono at $+3\%$, $\delta = 0.7$ in
$+4\%$, $\delta = 0.7$ in

Strips are not shown for clarity

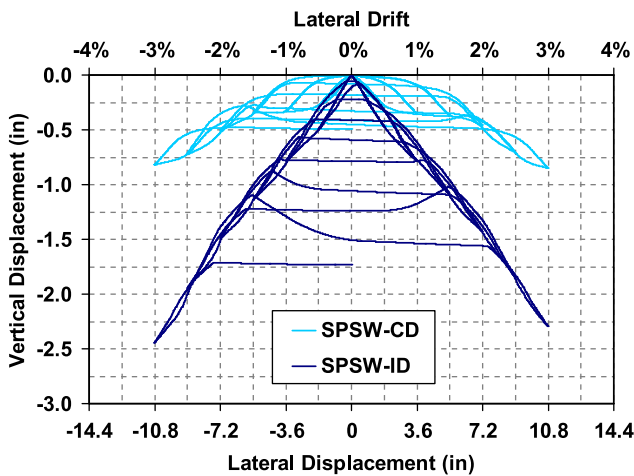**Fig. 6.** Schematic deformed shapes of (a) SPSW-ID; (b) SPSW-CD



**Fig. 7.** History of HBE3 vertical displacement (cyclic pushover)

actually occurred on the HBEs during cyclic pushover analysis. The largest HBE vertical deformation is 1.1 in. at $+3\%$ lateral drift. However, this is not large enough to create in-span plastic hinging and becomes only 0.5 in. (shown in Fig. 7 for HBE3) when the structure returns to its original position.

The complete history of vertical displacements of HBEs as a function of structure lateral drift, as shown in Fig. 7, is also instructive to explain the performance of the HBEs designed by the two different approaches. This figure compares vertical displacement history at the midspan of the top HBE for both SPSWs, in terms

of (1) the maximum drift of every cycle (called the backbone displacement) and (2) when the structure returns to its original position at $0\%$ drift (called the residual displacement). The backbone-displacement slope of SPSW-ID is larger than that of SPSW-CD, implying that the HBE vertical downward displacement for SPSW-ID increases faster than that for SPSW-CD. In other words, this accumulative plastic incremental deformation attributable to cyclic pushover displacement detrimentally affects the structural performance of SPSW-ID. For example, at $+3\%$ drift, the HBE3 vertical displacement of SPSW-ID was 2.3 in., or approximately 2.6 times larger than that of SPSW-CD, which was 0.9 in. The same trend was also exhibited with the residual displacements. At the end of the 3% drift cycle, HBE3 residual displacement for the SPSW-ID was 3.5 times larger than that for the SPSW-CD. In addition, progression of the HBE residual displacement from one cycle to another cycle is quicker for the SPSW-ID than that for the SPSW-CD. Moreover, this phenomenon on SPSW-ID is even worse if a smaller W-section was been used for the top HBE such that its demand-to-capacity ratio was closer to 1.0. A value of 0.88 (as shown in Fig. 1) was obtained for that top HBE in the SPSW-ID case compared with the corresponding 0.99 value at the top HBE of SPSW-CD. If anything, this discrepancy reinforces the conclusions reached by this case study.

**Moment-Rotation Comparison.** Another approach that can be used to examine the behavior of the two SPSWs is comparing the moment-rotation hysteresis of their HBEs, as in Fig. 8, which plots the normalized moment-rotation hysteresis of each HBE (arranged vertically from the top to the bottom HBE) obtained during the cyclic pushover displacements. The normalized terms plotted are $M/Mp$ and $\theta/\theta_{0.03}$, where $M$ and $Mp$ = end moment
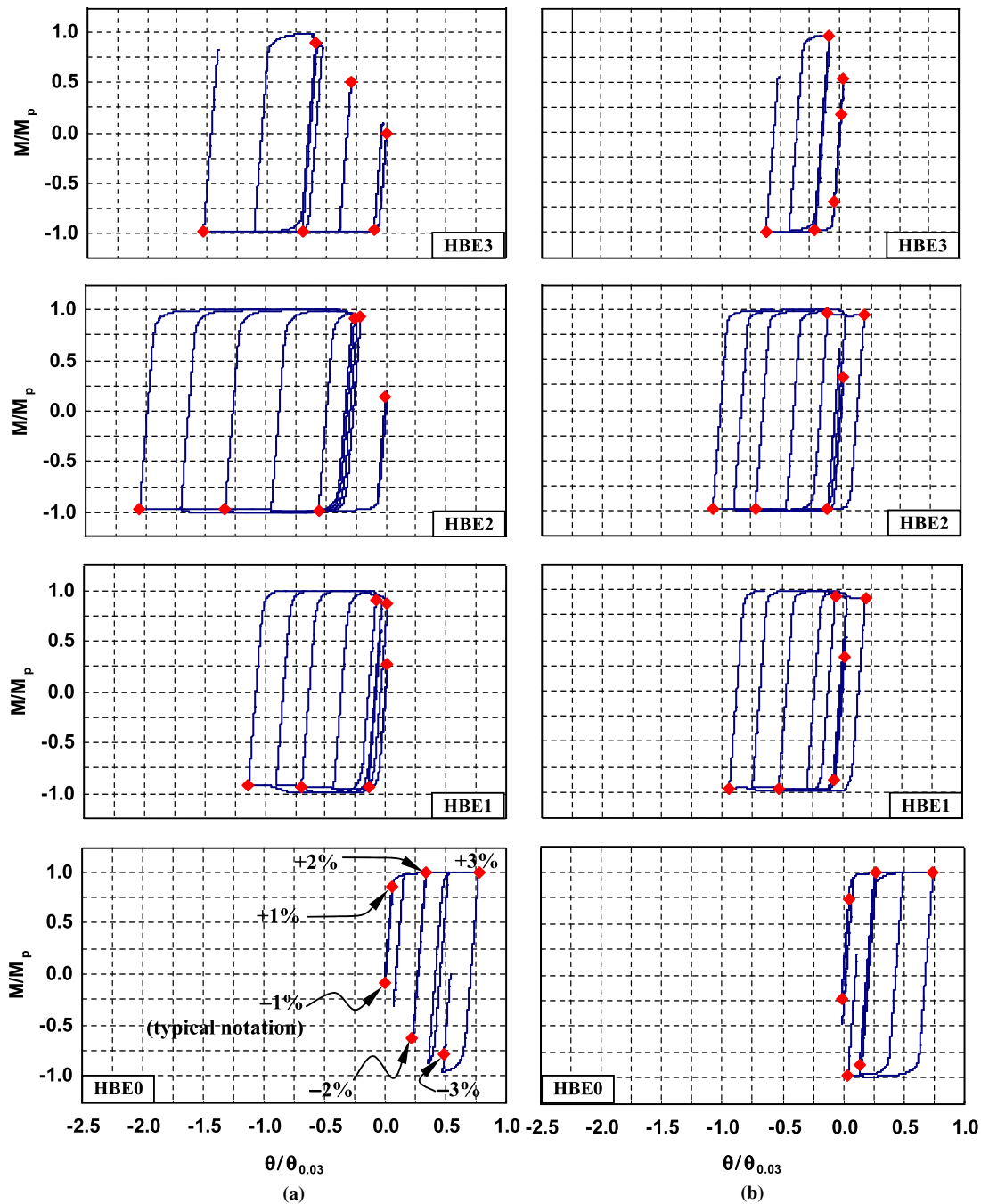
**Fig. 8.** Normalized moment-rotation hysteresis at HBE left end for (a) SPSW-ID; (b) SPSW-CD

and the corresponding HBE plastic moment capacity, respectively, and $\theta$ and $\theta_{0.03}$ = angle of rotation and the required plastic rotation capacity of a special moment-resisting frame, often specified as equal to 0.03 radians (Bertero et al. 1994; SAC 1995). Diamond markers included on each hysteretic curve correspond to the normalized values reached at lateral drifts of positive and negative 1, 2, and 3%, as indicated in Fig. 8. The hysteretic curves of both HBE ends are somewhat similar, except that they are the mirror image of one another, and thus only those of the HBE left end are presented.

Unlike the general hysteresis curve for special moment-resisting frames, which is typically symmetric with respect to positive and negative rotations developed under a symmetric cyclic pushover

displacement history, the hysteresis curves of both SPSWs considered in this paper are not symmetric but looping with a bias toward one direction. The curve loops toward the positive side for the bottom HBE and to the negative side for the other HBEs, where positive and negative rotations are respectively defined as corresponding to tension on the bottom and top side of the HBE. The tension forces from the infill plates contribute to this behavior by always pulling the HBE in the direction of the tension forces (i.e., pulling the bottom HBE up and the other HBEs down). Interestingly, except for the bottom HBE, all the moment-resisting ends of the HBEs of SPSW-ID developed a cross-section rotation (i.e., cross-section curvature multiplied by plastic hinge length) greater than 0.03 radians after the structure was pushed cyclically up to a
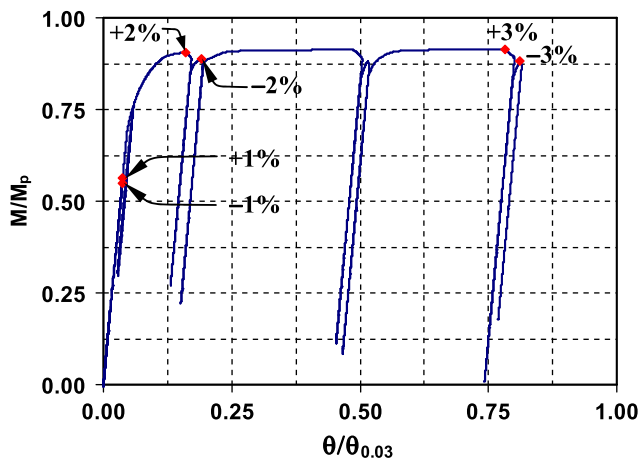
**Fig. 9.** Normalized moment-rotation hysteresis at midspan of HBE2

maximum lateral drift of 3%. In one case (i.e., HBE2), the total rotations even reached 0.062 radians. Such a significantly high cyclic rotation demand would be difficult to achieve using the type of moment-resisting connections used in SPSW (the AISC 2005 Seismic Specifications only require that ordinary-type connections be used in SPSW). In fact, the significantly high cyclical rotation demand might also be difficult to achieve with special moment-resisting frame (SMRF) beam-to-column connections approved by AISC 2005, which are experimentally verified to perform well up to ±0.04 radians total rotations or ±0.03 radians plastic rotations. By comparison, for SPSW-CD, all HBE total rotations obtained were less than or equal to 0.03 radians under the same cyclic pushover displacements up to 3% drift.

In light of the specific system behavior observed, investigating the moment-rotation hysteresis at a typical location at which in-span plastic hinge occurred was also of interest. For this purpose, this was done for HBE2 of SPSW-ID, which is the HBE that developed the largest total rotations at its end [Fig. 8(a)] in the example considered; its normalized moment-rotation hysteresis at the midspan (i.e., the location of in-span plastic hinge) is shown in Fig. 9. Knowing that significant accumulation of plastic incremental deformations occurred in SPSW-ID, one might have expected in-span plastic hinge rotations comparable in magnitude with that of the plastic hinge at the right end of HBE2. However, the result presented in Fig. 9 contradicts that expectation. The flexibility of HBE2 primarily contributed to this phenomenon. As shown in Fig. 6(a) for the deformed shape of SPSW-ID, because of elastic deformations, the slope at the midspan of HBE2 (the location of the in-span plastic hinge) was relatively small and no obvious kink was observed. For comparison, a case study conducted in which rigid members were assigned to all HBEs except at the location of fiber hinges whereas the other analytical model properties remained the same as previously presented verified that the total rotations at the midspan indeed approached 0.06 radians.

An interesting behavior observed in the hysteresis curve of Fig. 9 is its creeping behavior, meaning that the rotation never comes back to zero, unlike what was observed in the end-span hinges (Fig. 8), but rather gradually increases regardless of the direction of the cyclic pushover displacement. In this case, the rotations were 0.002, 0.006, and 0.024 radians at the end of the 1, 2, and 3% cycles, respectively. The normalized moment reached a maximum value of $0.92M_p$, attributable to the significant axial force developed at midspan of HBE2 (i.e., $P = 25\%P_y$).

From an overall perspective, although failures of HBE to VBE connections have been few in SPSW tested at the time of this

writing, these results might also suggest that large drift may translate into large plastic rotations even for SPSW-CD. However, before mandating the use of SMRF connection for HBEs to VBEs, it is important to recognize that the plastic rotations demands observed here were not symmetric, by contrast with moment frame behavior. In other words, a SPSW-CD HBE rotation demand of $+0.0075$ to $-0.03$ radians is less critical than a SMRF beam rotation demand of $\pm0.03$ radians. However, the SPSW-ID HBE rotation demands of 0.0 to 0.06 radians may approach that of the SMRF. More research is desirable in this regard.

## Nonlinear Time-History Analysis

Whereas several key seismic behaviors of steel plate shear walls with HBEs designed to have different plastic mechanisms have been discovered through the incrementally cyclic pushover analysis, conducting nonlinear time-history analysis remains necessary to investigate whether those previous results would be replicated during earthquake excitations and whether additional seismic behaviors for the aforementioned SPSW systems would emerge as a consequence of the random nature of earthquake records. This verification is also important given that unstiffened web plates can only yield in tension (i.e., requiring greater drifts to yield more).

Three synthetic time histories of ground acceleration were generated for this purpose using the computer code TARSCTHS (Papageorgiou et al. 1999) for specified target response spectra, moment magnitude of seismic source, and site-to-source distance. TARSCTHS-generated strong motions accurately match any user-specified spectra, which allow investigation of inelastic time-history behavior considering a small number of earthquake excitations that can simulate with high fidelity the demands anticipated for the specified target design spectra. The target response spectra was the previously discussed design basis earthquake (DBE) response spectra and generated only up to the period of 2.5 s, which corresponded with the largest possible theoretical value of the fundamental period for the considered SPSWs (this value was estimated for the condition after the infill plates of SPSW-ID stretched during yielding and thus stopped contributing to the wall stiffness, and considering only the contribution of the boundary frames for lateral resistance). The moment magnitudes of the three synthetic ground motions denoted as SYNT1, SYNT2, and SYNT3 were 6.5, 7.0, and 7.5, respectively, with corresponding site-to-source distances of 11, 18, and 25 km. They were generated to last up to 25 s, with approximately 15 s of strong motions. The peak ground accelerations (PGA) of these synthetic ground motions were 0.51, 0.63, and 0.59 g for SYNT1, SYNT2, and SYNT3, respectively.

### Analysis Results

In general, each synthetic ground motion produced somewhat the same maximum deformation and residual deformation for a given HBE in a given SPSW, but values were smaller for SPSW-CD than for SPSW-ID. The governing ground motion (as per the ASCE 7-05 definition) is SYNT2 and the results obtained from this ground motion on HBE3 (which experienced the largest deformations) are predominantly used in the following discussion.

The complete histories of HBE3 vertical deformation both for SPSW-ID and SPSW-CD are plotted in Fig. 10. The accumulative plastic incremental deformation is still observed, with maximum and residual vertical deformations more apparent on SPSW-ID than on SPSW-CD. For example, when SPSW-CD reached a lateral drift of 1% for the first time (point A in Fig. 10), the largest HBE3 vertical displacement at the same drift for SPSW-ID (point A')
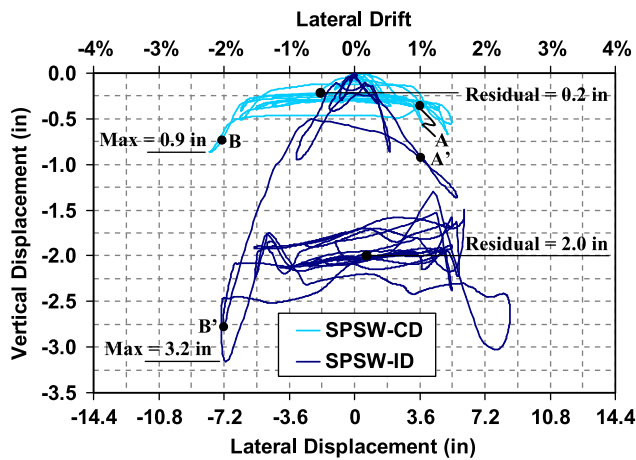
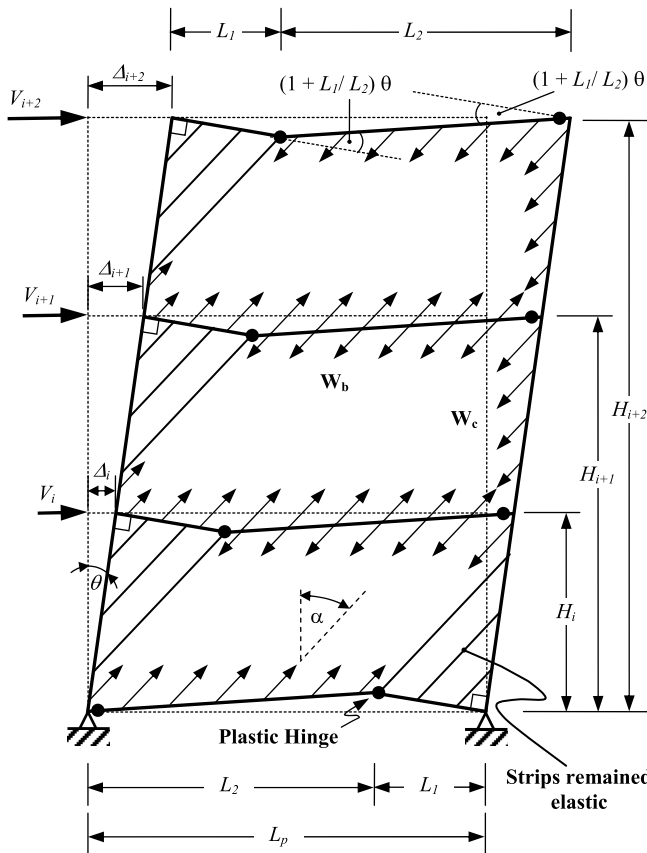**Fig. 10.** History of HBE3 vertical displacement (time history)



**Fig. 11.** Sway and beam combined plastic mechanism for multistory SPSW

was 2.25 larger (those two 1% drift conditions did not occur at the same time). As the ground excitation increased and caused a 2% lateral drift on both structures for the first time, the difference between the two became four times larger (points B and B'). This implies that the HBE3 vertical downward displacement for SPSW-ID increased faster than that for SPSW-CD as the lateral drift increased. Moreover, the same trend was exhibited for the maximum vertical displacement (0.9 in. versus 3.2 in.) and the residual vertical displacement at the end of the record (0.2 in. versus 2.0 in.). The maximum vertical displacements for SPSW-CD and SPSW-ID did not occur at the same lateral drift.

A careful examination of the SYNT2 ground motion input was conducted to investigate whether anything in it could be attributed to cause the jump from point A' to B' (i.e., why the vertical deformation of HBE3 significantly increases from 0.93 in. at $+1\%$ drift to 2.78 in. at $-2\%$ drift within a single yield excursion). This synthetic ground motion is similar to typical far-field earthquake records in which peak acceleration values of strong motions occurred several seconds after the initial motion, fluctuated with a number of cycles reaching approximately the same peak acceleration magnitude for several seconds, and decayed toward the end of the record. Though within the strong motion times corresponding to displacements A' to B' SYNT2 contains accelerations higher than 0.4 $g$, nothing unusual was observed in the ground motion. Specifically, no distinct acceleration spike or pulselike condition similar to what could be typically encountered on near-fault ground motions was observed within this region and could be inferred to be responsible for this behavior. In addition, randomness of the ground motion within this region is somewhat similar to other parts of the SYNT2 ground motion signature. Note that the same behavior for SPSW-ID was also observed during the excitation of the other two ground motions (i.e., SYNT1 and SYNT3).

Table 1 shows that the maximum vertical deformation for HBE3 of SPSW-ID obtained from the nonlinear time-history analysis is 1.8 times higher than that obtained from the cyclic pushover analysis, whereas for the other HBEs of both SPSWs, the magnitudes are relatively similar. To ensure a consistent comparison, information in Table 1 for the cyclic pushover analysis was obtained at the maximum drift that occurred during the nonlinear time-history analysis (i.e., at 2.4 and 2.2% drift for SPSW-ID and SPSW-CD, respectively).

The nonlinear time-history analyses were then extended to investigate the performance of both SPSWs under the more severe maximum considered earthquake (MCE) again using TARSCTHS to generate synthetic ground-motion histories with moment magnitudes and site-to-source distances similar to those in the DBE case but whose response spectra matched the MCE target spectra (for which vertical ordinates are 1.5 times greater than the DBE target spectra). To distinguish from the DBE case, the resulting three synthetic ground motions are denoted as SYNT4, SYNT5, and SYNT6. Their PGA-generated only upgenes were 0.81,

**Table 1.** HBE Maximum Vertical Deformation Obtained from Cyclic Pushover Analysis and Nonlinear Time-History Analyses

| Location of HBE | SPSW-ID | | | SPSW-CD | | |
|---|---|---|---|---|---|---|
| | $\delta_{\max-CP}$[a] (in.) | $\delta_{\max-TH-DBE}$[b] (in.) | $\delta_{\max-TH-MCE}$[c] (in.) | $\delta_{\max-CP}$[a] (in.) | $\delta_{\max-TH-DBE}$[b] (in.) | $\delta_{\max-TH-MCE}$[c] (in.) |
| HBE-3 | 1.8 | 3.2 | 5.1 | 0.7 | 0.9 | 0.9 |
| HBE-2 | 2.5 | 2.7 | 4.6 | 1.1 | 1.1 | 1.4 |
| HBE-1 | 1.4 | 1.5 | 1.9 | 0.9 | 0.9 | 1.2 |
| HBE-0 | 1.0 | 0.9 | 1.5 | 0.6 | 0.4 | 0.7 |

[a]HBE maximum vertical deformation occurred at 2.4 (SPSW-ID) and 2.2% drift (SPSW-CD).
[b]Range of drifts (SYNT2): $-2.1$ to $+2.4$ (SPSW-ID) and $-2.2$ to $+1.5\%$ (SPSW-CD).
[c]Range of drifts (SYNT5): $-2.7$ to $+4.0$ (SPSW-ID) and $-3.4$ to $+3.2\%$ (SPSW-CD).

0.79, and 0.82 $g$ for the respective synthetic ground motions. In this paper, the governing ground motion is SYNT5, which created the largest vertical deformation on HBE3. As shown in Table 1, as the severity of the synthetic ground motions increased for the MCE case (consequently generating higher lateral drifts on both SPSWs), HBE vertical deformations of SPSW-ID especially at the top two floors significantly increased compared with the corresponding magnitudes in the DBE case. For example, HBE3 maximum vertical deformation increased from 3.2 in the DBE case to 5.1 in. in the MCE case. By comparison for SPSW-CD, only minor changes of HBE vertical deformations occurred. Hence, when formation of in-span plastic hinges on HBEs is possible, such as in the case of SPSW-ID, the more severe the ground excitations, the more accumulation of plastic incremental deformation observed.

## Conclusions

A case study investigating the seismic behavior of two steel plate shear walls with boundary elements designed according to different philosophies, was conducted. A common design approach encountered in practice, the indirect capacity design approach, was used to design the first shear wall (SPSW-ID). This approach does not guarantee that formation of in-span plastic hinges on horizontal boundary elements will be prevented. The second shear wall (SPSW-CD) was designed by the capacity design approach, which guarantees that plastic hinges can only occur at the ends of HBEs. Note that conclusions on the behavior of the SPSW-ID are equally applicable to SPSWs designed by any method for which in-span hinges are not explicitly prevented.

Monotonic and cyclic pushover analyses and nonlinear time-history analyses were conducted to investigate behavior. Plastification along HBE spans (i.e., in SPSW-ID) was demonstrated to induce significant accumulation of plastic incremental deformations on the HBEs, themselves leading to partial yielding of the infill plates and correspondingly lower global plastic strength compared with the values predicted by code equations (i.e., AISC 2010). In addition, in-span hinging in SPSW-ID caused total (elastic and plastic) HBE rotations greater than 0.03 radians after the structure was pushed cyclically up to a maximum lateral drift of 3%. Nonlinear time-history analysis also demonstrated that increasing the severity of the ground excitations (i.e., from DBE to MCE) accentuated the accumulation of plastic incremental deformations on the HBEs of SPSW-ID, whereas this was not the case for SPSW-CD. The plastic mechanism diagram (in Appendix I) suggests that the observed behaviors are possible, irrespective of the number of stories.

This paper establishes the various potential consequences of in-span hinging, which is an essential starting point to guide future discussions on the topic given the observed current trends in optimizing SPSW design. Future research is needed to assess how the magnitude of the preceding consequences varies as a function of various parameters and to investigate whether bounds exist within which the preceding behaviors are not likely to occur. Such parametric studies could include various structure configurations (i.e., number of stories, different infill plate aspect ratios and plate thickness, and relative stiffness between anchor beams and intermediate HBEs), various kinds of steel models (i.e., incorporate strain hardening, overstrength, material deterioration), different levels of gravity loads, and various ground-motion characteristics and variability. In addition, experimental verification would be desirable. The results and behavior presented obtained using simple plastic theory (as commonly done in similar studies), provide a first anchor point from which the effect of multiple other circumstances can be assessed.

Finally, an unanticipated valuable observation of this study was that the cyclic hysteretic moment-rotation curve of plastic hinges at the ends of HBEs are not symmetric, even in SPSWs that do not develop in-span hinging. These curves loop with a bias without sign reversal of the rotations, resulting in maximum rotations of significant magnitude. Past research has typically not quantified plastic hinge rotation histories and, in light of the results reported, this subject should deserve more attention in future research.

## Appendix I. Plastic Analysis of SPSW with In-Span Plastic Hinge

The kinematic method of plastic analysis is used to calculate the theoretical ultimate strength of a SPSW considering that plastic hinges can develop along the span of HBEs (rather than just at their ends), as observed to occur in the SPSW-ID case. A sway and beam combined plastic mechanism is used, instead of the uniform plastic sway mechanism considered in Berman and Bruneau (2003). This combined plastic mechanism is schematically shown in Fig. 11 for a multistory SPSW. A solution is obtained by equating the plastic internal work and external work.

When the applied shear force at every story $V_i$ displaces the corresponding floor by a magnitude $\Delta_i$, the generated tension forces in the infill plates cause plastic hinges to develop both at the HBE end and along its span. As a result, some of the infill plates remain elastic. The total external work ($W_{external}$) is the summation of works produced by each shear force $V_i$ as follows:

$$W_{external} = \sum_{i=1}^{n_s} V_i \Delta_i = \sum_{i=1}^{n_s} V_i H_i \theta \tag{4}$$

where $H_i$ = height from the base to the $i$th story; $n_s$ = total number of stories; and $\theta$ = angle between the deformed structure and the vertical, which is also equal to the top HBE lateral displacement over the total height of the structure.

Work done by the plastic hinges on the HBEs and by the strips contributes to the internal work ($W_{internal}$). The total internal work produced by the first component can be calculated as follows:

$$W_{internal\_1} = 2 \sum_{i=0}^{n_s} M_{pbi} \left(1 + \frac{L_1}{L_2}\right) \theta \tag{5}$$

where $M_{pbi}$ = plastic moment of HBE at the $i$th story, with each HBE having two plastic hinges, and $L_1$ and $L_2$ are as shown in Fig. 11. Note that because a strong-column weak-beam design approach is mandated in the design of SPSW, plastic hinges are assumed to develop in the HBEs.

As for the internal work done by the strips, only work by the yielding infill plates is included (the contribution from the elastic infill plates is neglected, as all other elastic work in accordance with plastic theory). To calculate the strips contribution, using the horizontal and vertical components of the strip yield forces is easier. The vertical and horizontal component of the strip yield forces

on the VBEs are denoted as $W_{yc}$ and $W_{xc}$, respectively; whereas on the HBEs, they are denoted as $W_{yb}$ and $W_{xb}$ for the same respective components. Because the vertical deformation on the VBEs is negligible, $W_{yc}$ on the VBEs produces no internal work. Although the $W_{xc}$ does produces internal work, the $W_{xc}$ on the left and right VBE produce negative and positive internal work, that practically cancel one another (Berman and Bruneau 2003). Therefore, only the $W_{xb}$ and $W_{yb}$ components on the HBEs produce internal work. The strip

yield forces acting on the anchor beams (i.e., the top and bottom HBEs) produce positive internal work, whereas the forces acting on the intermediate HBEs produce both positive and negative work (i.e., the strip yield forces acting on the bottom of an HBE at a particular story produce positive internal work, whereas the strip forces acting on top of the same HBE produce negative internal work, as shown in Berman and Bruneau 2003). Thus, the total internal work produced by the yielding strips is

$$W_{\text{internal\_2}} = \underbrace{\sum_{i=1}^{n_s} \frac{1}{2} F_{yp}(t_{wi}L_2 - t_{wi+1}L_p) \sin(2\alpha)H_i\theta}_{\text{Horizontal component of the strip yield forces}} + \underbrace{F_{yp}t_{w1}L_2\cos^2\alpha\frac{L_1}{2}\theta + \sum_{i=1}^{n_s} F_{yp}(t_{wi}L_2 - t_{wi+1}L_p)\cos^2\alpha\frac{L_1}{2}\theta}_{\text{Vertical component of the strip yield forces}} \qquad (6)$$

where all parameters are as defined previously. Equating the external and internal work [Eqs. (4)–(6)] gives the following general equation to calculate the ultimate strength of multistory SPSW with combined mechanism:

$$\sum_{i=1}^{n_s} V_iH_i = \underbrace{2\left(\frac{L_p}{L_p-L_1}\right)\sum_{i=0}^{n_s} M_{pbi}}_{\text{Plastic Hinge on the HBEs}} + \underbrace{\sum_{i=1}^{n_s} \frac{1}{2} F_{yp}L_p(t_{wi} - t_{wi+1})\sin(2\alpha)H_i - \sum_{i=1}^{n_s} \frac{1}{2} F_{yp}t_{wi}L_1\sin(2\alpha)H_i}_{\text{Horizontal component of the strip yield forces}}$$

$$+ \underbrace{F_{yp}t_{w1}L_2\cos^2\alpha\frac{L_1}{2} + \sum_{i=1}^{n_s} F_{yp}(t_{wi}L_2 - t_{wi+1}L_p)\cos^2\alpha\frac{L_1}{2}}_{\text{Vertical component of the strip yield forces}} \qquad (7)$$

At this point, the distance of the in-span plastic hinge $L_1$ needs to be determined. One could obtain the exact location of that hinge by setting the first derivative of Eq. (7) to zero. An iterative procedure could also be used by assuming a trial value for $L_1$ and iterating (increasing or decreasing $L_1$) until accurate results are obtained (i.e., lowest calculated ultimate strength). However, these approaches are cumbersome. An easier approach is to take advantage of the SAP2000 results already obtained. As shown in Figs. 3 and 5, the location of in-span plastic hinges is at about a quarter-span except for the second floor HBE (labeled HBE2), where it is at about midspan. Moreover, there is no need to achieve high accuracy of in-span plastic hinge location because designing SPSWs with HBEs having in-span hinges is not advisable.

## Appendix II. Finite Element Validation of SPSW-ID Behavior

To validate the development of HBE in-span plastic hinges previously observed on SPSW-ID, a finite-element (FE) monotonic pushover analysis of this structure [Fig. 1(a)] was conducted. The commercially available software ABAQUS/Standard (ABAQUS/Standard Version 6.9-1) was used for this purpose. The entire infill plate and boundary elements (HBEs and VBEs) were meshed using the S4R shell elements isoparametric general-purpose four-node shell element with reduced integration and hourglass control. The resulting FE model contained 32,244 shell elements with an average dimension of $2 \times 2$ in. per shell element. The exterior nodes of the HBE flange elements and around the perimeter of the panel zones were restrained against out-of-plane movement to replicate lateral supports.

Fig. 12 shows the finite-element analysis results at 4% lateral drift. In addition to plastic hinges that occurred at the HBE ends,

in-span plastification occurred at each HBE similar to that previously observed using strip model of SAP2000 [Fig. 3(a)]. As indicated in Fig. 12, elastic tension field action is observed in some
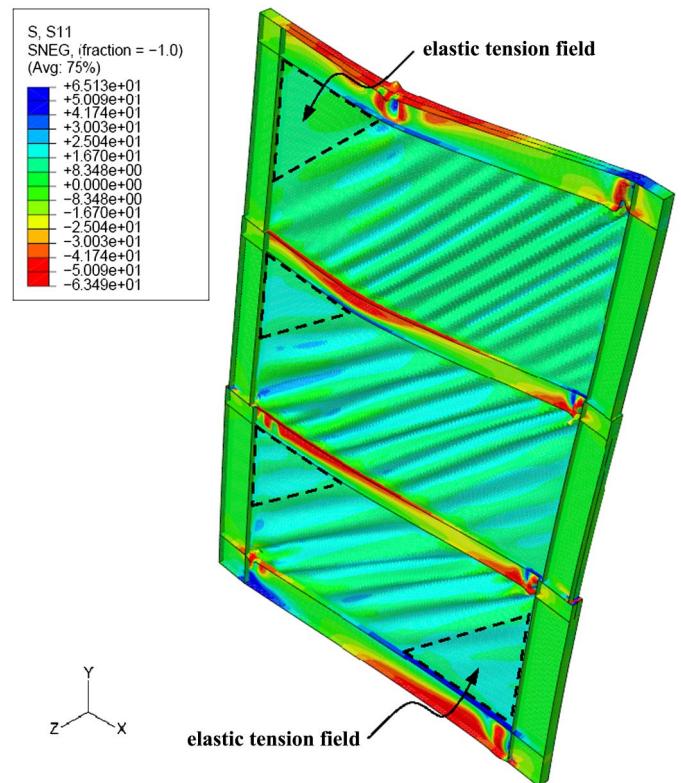


**Fig. 12.** FEA validation of SPSW-ID behavior (at 4% drift)

parts of the infill plates. Moreover, the ultimate base shear strength is 296 kips, which agrees within 2.6% with the theoretical base shear for SPSW-ID per Eq. (7).

## References

*ABAQUS/Standard Version 6.9-1* [Computer software]. Hibbitt, Karlsson, and Sorenson (HKS), Pawtucket, RI.

AISC. (2005). "Seismic provisions for structural steel buildings." *ANSI/AISC 341-05*, Chicago.

AISC. (2007). "Modern steel construction." *AISC Magazine*, January 2007 (cover page photo).

AISC. (2008). "L.A. live hotel and residences: An innovative steel-plate shear wall solution." ⟨http://www.aisc.org/content.aspx?id=16012⟩ (Oct. 2008).

AISC. (2010). "Seismic provisions for structural steel buildings." *ANSI/AISC 341-10*, Chicago.

Berman, J. W., and Bruneau, M. (2003). "Plastic analysis and design of steel plate shear walls." *J. Struct. Eng.*, 129(11), 1448–1456.

Berman, J. W., and Bruneau, M. (2005). "Experimental investigation of light-gauge steel plate shear walls." *J. Struct. Eng.*, 131(2), 259–267.

Berman, J. W., and Bruneau, M. (2008). "Capacity design of vertical boundary elements in steel plate shear walls." *Eng. J.*, 45(3), 57–71.

Bertero, V. V., Anderson, J. C., and Krawinkler, H. (1994). "Performance of steel building structures during the Northridge earthquake." *Rep. No. UCB/EERC-94/09*, Earthquake Engineering Research Center, Univ. of California, Berkeley, CA.

Bruneau, M., Whittaker, A. S., and Uang, C. M. (1998). *Ductile design of steel structures*, McGraw-Hill, New York.

Caccese, V., Elgaaly, M., and Chen, R. (1993). "Experimental study of thin steel plate shear walls under cyclic load." *J. Struct. Eng.*, 119(2), 573–587.

Driver, R. G., Kulak, G. L., Elwi, A. E., and Kennedy, D. J. L. (1998). "FE and simplified models of steel plate shear walls." *J. Struct. Eng.*, 124(2), 121–130.

Driver, R. G., Kulak, G. L., Kennedy, D. J. L., and Elwi, A. E. (1997). "Seismic behavior of steel plate shear walls." *Structural Engineering Rep. 215*, Dept. of Civil Engineering, Univ. of Alberta, Edmonton, Alberta, Canada.

Elgaaly, M. (1998). "Thin steel plate shear walls behavior and analysis." *Thin-Walled Struct.*, 32(1–3), 151–180.

FEMA. (2003). "NEHRP recommended provisions for seismic regulations for new buildings and other structures." *FEMA Rep. No. 450*, Building Seismic Safety Council for FEMA, Washington, DC.

Lopez-Garcia, D., and Bruneau, M. (2006). "Seismic behavior of intermediate beams in steel plate shear walls." *Proc., 8th U.S. National Conf. on Earthquake Engineering* (CD-ROM), Earthquake Engineering Research Institute (EERI), El Cerrito, Calif.

Papageorgiou, A., Halldorsson, B., and Dong, G. (1999). "Target acceleration spectra compatible time histories." *TARSCTHS user's manual*, State Univ. of New York at Buffalo, Buffalo, NY.

Purba, R., and Bruneau, M. (2010). "Impact of horizontal boundary elements design on seismic behavior of steel plate shear walls." *Tech. Rep. MCEER-10-0007*, Multidisciplinary Center for Earthquake Engineering Research, State Univ. of New York at Buffalo, Buffalo, NY.

Qu, B., and Bruneau, M. (2008). "Seismic behavior and design of boundary frame members of steel plate shear walls." *Tech. Rep. MCEER-08-0012*, Multidisciplinary Center for Earthquake Engineering Research, Buffalo, NY.

Qu, B., and Bruneau, M., (2009). "Design of steel plate shear walls considering boundary frame moment resisting action." *J. Struct. Eng.*, 135(12), 1511–1521.

Qu, B., Bruneau, M., Lin, C. H., and Tsai, K. C. (2008). "Testing of full scale two-story steel plate shear walls with reduced beam section connections and composite floors." *J. Struct. Eng.*, 134(3), 364–373.

Sabelli, R., and Bruneau, M. (2007). *Design guide 20: Steel plate shear walls*, AISC, Chicago.

SAC. (1995). "Interim guidelines: Evaluation, repair, modification and design of welded steel moment frame structures." *Program to Reduce the Earthquake Hazards of Steel Moment Frame Structures, Rep. FEMA 267/SAC-95-02*, SAC Joint Venture, Sacramento, CA.

*SAP2000 Version 11.0.8* [Computer software]. Computer and Structures, Berkeley, CA.

Thorburn, L. J., Kulak, G. L., and Montgomery, C. J. (1983). "Analysis of steel plate shear walls." *Structural Engineering Rep. No. 107*, Dept. of Civil Engineering, Univ. of Alberta, Edmonton, Alberta, Canada.

Timler, P. A., and Kulak, G. L. (1983). "Experimental study of steel plate shear walls." *Structural Engineering Rep. No. 114*, Dept. of Civil Engineering, Univ. of Alberta, Edmonton, Alberta, Canada.

Vian, D., and Bruneau, M. (2005). "Steel plate shear walls for seismic design and retrofit of building structures." *Tech. Rep. MCEER-05-0010*, Multidisciplinary Center for Earthquake Engineering Research, State Univ. of New York at Buffalo, Buffalo, NY.